Energy Conversion and Management 287 (2023) 117061

Contents lists available at ScienceDirect

Energy Conversion and Management

journal homepage: www.elsevier.com/locate/enconman

A unified framework for the thermo-economic optimisation of compressed-air energy storage systems with solid and liquid thermal stores

Matthias Mersch [a,b,c], Paul Sapin [a,b], Andreas V. Olympios [a,b], Yulong Ding [d], Niall Mac Dowell [b,c], Christos N. Markides [a,b,*]

[a] Clean Energy Processes (CEP) Laboratory, Department of Chemical Engineering, Imperial College London, London SW7 2AZ, UK
[b] Centre for Process Systems Engineering (CPSE), Department of Chemical Engineering, Imperial College London, London SW7 2AZ, UK
[c] Centre for Environmental Policy, Imperial College London, London SW7 2AZ, UK
[d] Birmingham Centre of Energy Storage (BCES) & School of Chemical Engineering, University of Birmingham, Birmingham B15 2TT, UK

ARTICLE INFO

Keywords:
Compressed air energy storage
Inter-seasonal grid-scale energy storage
Packed-bed
Techno-economic optimisation
Thermal storage
Thermo-mechanical energy storage

ABSTRACT

Compressed-air energy storage is an attractive option for satisfying the increasing storage demands of electricity grids with high shares of renewable generation. It is a proven technology that can store multiple gigawatt hours of electricity for hours, days and even weeks at a competitive cost and efficiency. However, compressed–air energy storage plants need to be designed carefully to deliver these benefits. In this work, a consistent thermo-economic optimisation framework is applied to assess the performance and costs of different compressed–air energy storage configurations across different scales. Special attention is paid to the thermal energy stores, with both solid packed-bed stores and liquid stores examined as viable options for advanced compressed–air energy storage plants and different storage materials proposed for both options. The comprehensive thermo-economic optimisation, considering different system layouts, thermal energy storage technologies and storage materials, and system scales is a key novelty of the presented work. A configuration with two packed–bed thermal energy stores using Basalt as the storage material is found to perform best, achieving an energy capital cost of 140 $/kWh, a power capital cost of 970 $/kW and a roundtrip efficiency of 76% at a nominal discharge power of 50 MW and a charging / discharging duration of 6 h. The best-performing liquid storage material is solar salt, which is associated with an energy capital cost of 170 $/kWh and a power capital cost of 1,230 $/kW. Systems with liquid thermal energy stores however are found generally to perform worse than systems with packed–bed thermal energy stores both in terms of cost and efficiency across all scales.

1. Introduction

Renewable energy sources (RESs) account for a steadily increasing share of electricity generation across the globe [1], driven by decreasing investment costs, low marginal costs, the need to reduce emissions and to meet environmental and climate targets, and the strive for increased energy autarky. However, increased penetration of RESs is associated with challenges for energy systems. Due to the intermittent nature of RESs, additional efforts are required to ensure grid stability and power supply security.

Increased power system flexibility is essential for an efficient integration of large capacities of non-dispatchable RES generation [2]. This can be achieved in many ways, including increased flexibility of dispatchable conventional power plants, demand-side management, strategic curtailment, smart grids and energy storage systems (ESSs) [3], as well as dynamic network reconfiguration, increased network interconnections and energy system integration [4]. Especially ESSs play an essential role in the integration of large shares of RES generation into energy systems, as they can balance non-dispatchable generation with in- or limited-flexible demand. This increases utilisation of RES generation capacity, reduces curtailing, and increases the overall share of electricity provided from RESs [5].

The role of energy storage in deeply decarbonised energy systems has been explored extensively in literature. De Sisternes et al. [6] investigated the value of energy storage in decarbonising the power system of the US state of Texas. They conclude that ESSs provide value by increasing the cost-effective penetration of RES generation; however, they compete with other low-carbon power generation technologies such as flexible nuclear. The value of ESS with a 2 h storage capacity is

* Corresponding author at: Clean Energy Processes (CEP) Laboratory, Department of Chemical Engineering, Imperial College London, London SW7 2AZ, UK.
E-mail address: c.markides@imperial.ac.uk (C.N. Markides).

https://doi.org/10.1016/j.enconman.2023.117061

Available online 29 April 2023

Nomenclature

Symbols

α	Heat transfer coefficient [W/m/K]
a	Parameter for Kaunas correlation [-]
b	Parameter for Kaunas correlation [-]
A	Area [m^2]
γ	Specific heat capacity ratio [-]
C	Cost [$]
c_p	Isobaric specific heat capacity [J/kg/K]
c_v	Isochoric specific heat capacity [J/kg/K]
C_R	Heat capacity flow ratio [-]
d	Diameter [m]
D_p	Pebble diameter [m]
Δt	Time step [s]
δ_w	Wall thickness [m]
Δx	Length increment [m]
∈	Void fraction [-]
ε	Heat exchanger effectiveness [-]
η	Efficiency [-]
h	Fin height [m]
η_p	Polytropic efficiency [-]
L_{tp}	Distance between tubes [m]
λ	Thermal conductivity [W/m/K]
J	Correction factor [-]
Nu	Nusselt number [-]
m	Fin efficiency parameter [1/m]
$\dot{m}$	Mass flowrate [kg/s]
NTU	Number of transfer units [-]
p	Pressure [Pa]
ρ	Density [kg/m^3]
ϕ	Fin efficiency [-]
ψ	Viscosity [Pa·s]
Pr	Prandtl number [-]
Re	Reynolds number [-]
s	Parameter for Kaunas correlation [-]
t	Time [s]
T	Temperature [K]
v	Superficial velocity [m/s]
v_m	Maximum fluid velocity [m/s]
$\dot{W}$	Work [J]
ϕ^r	Viscosity correction factor [-]

Subscripts/superscripts

cha	Charging
comp	Compressor
disc	Discharging
e	Effective
EC	Energy capital
el	Electric
f	Fin
g	Gas
i	Ideal
in	Inner/Inlet
m	Mean
PC	Power capital
r	Unfinned area
s	Solid
ss	Shell-side
t	Total
turb	Turbine
ts	Tube-side
out	Outer/Outlet
w	Wall

Abbreviations

A-CAES	Adiabatic CAES
CAES	Compressed-air energy storage
ESS	Energy storage system
L-TES	Liquid thermal energy store
LAES	Liquid-air energy storage
LCOS	Levelised-cost-of-storage
PB-TES	Packed-bed thermal energy store
PHS	Pumped-hydro storage
PTES	Pumped-thermal electricity storage
RES	Renewable energy source
ST-HEX	Shell-and-tube heat exchanger
TES	Thermal energy storage
TMES	Thermo-mechanical energy storage

found to be on-par with current technology costs only under strict emission reduction targets, while the value of 10 h storage is comparable to current pumped-hydro storage (PHS) costs. The authors conclude that ESSs are essential for decarbonisation strategies with high shares of RES generation, but not required if a mix of flexible, dispatchable low-carbon energy sources is deployed. Safaei and Keith [7] reach a similar conclusion, stating that only relatively small capacities of ESS are required for moderate emission reduction targets, while substantial bulk energy storage capacity is required in deep-decarbonisation scenarios without any availability of dispatchable zero-carbon technologies. Arbabzadeh et al. [5] show that ESSs can substantially increase emission reductions and reduce RES curtailing in deep decarbonisation scenarios for the US state of California. Denholm and Mai [8] investigated the required storage durations to unlock the benefits of ESS. They find that at RES penetration rates of 55%, the first 4 h of storage duration add the largest benefit, while with 8 h of storage duration already half of the maximum possible avoided-curtailment benefits can be reached. The authors conclude that, at the investigated RES penetration rates, very-long duration or seasonal storage provides only little incremental value. Jafari et al. [9] also find that longer-duration ESSs have a lower marginal value per added storage capacity. ESSs with storage durations of 10 to 100 h only show a modest marginal value, while systems with storage durations of less than 10 h were found to add significant value. The authors also show that ESSs can significantly reduce the costs of decarbonising the Italian energy system if projected technology cost reductions are achieved.

From the literature it is apparent that ESS need to be cheap in order to be competitive, and storage durations of a few hours appear to provide the largest benefits to energy systems with a high penetration of RES generation. Many different ESS technologies have been developed and proposed, and plenty of review papers have been published. Chen et al. [10] introduce and categorise a variety of electric energy storage systems and provide key performance indicators. Koohi-Fayegh and Rosen [11] provide a more recent update. Aneke and Wang [12] also consider thermal energy storage and focus on real life applications, while Amirante et al. [13] also include hydrogen technologies. Gür [14] provides a very detailed description of various battery technologies. Luo et al. [15] provide recommendations for different applications of energy storage in power systems.

PHS is the traditional technology used for large-scale long-duration electricity storage, as it is cheap, reliable, efficient and offers long lifetimes. However, PHS is only possible in specific geographical locations and potential to increase capacities is limited to regions with suitable topology [16]. Additionally, the ecological impact of PHS is significant

[17]. Thermo-mechanical energy storage (TMES) systems and batteries are seen as the most promising alternatives for large-scale electricity storage. Both can reach the required power capacities of 10's of MWs and discharge durations of multiple hours. Despite recent technological advancements, batteries still face significant challenges. Lead-acid batteries, one of the most widely used type, suffer from short lifetimes. Li-ion batteries are more durable, have a high energy density and achieve high roundtrip efficiencies, but costs are still high and battery management is a challenge. Flow batteries are a promising technology for large-scale energy storage, as they offer easy scalability and decouple power and energy ratings [14]. However, the systems are complicated and expensive compared to other ESSs [15]. TMES combine elements of mechanical and thermal energy storage systems. Compressed-air energy storage (CAES) is a proven technology that can achieve low capital costs and roundtrip efficiencies of up to 70% when integrated with thermal energy storage (TES) systems [18]. Other TMES technologies are liquid–air energy storage (LAES) and pumped-thermal electricity storage (PTES), which are compared by Georgiou et al. on a technology [19] and whole-energy system [20] level. White et al. [21] present a thermodynamic analysis of PTES systems, analysing different sources of irreversibility and concluding that the ratio between highest and lowest temperature is most relevant for the cycle performance. In a recent study by McTigue et al. [22], it is found that roundtrip efficiencies greater than 60% are possible with PTES, while costs are competitive with Li-ion batteries. Zhao et al. [44] determined a maximum roundtrip efficiency of 68% for a transcritical CO_2 PTES system, and minimum energy capital cost of about 400 $/kWh. For a comprehensive review of TMES the reader is referred to Olympios et al. [18].

CAES systems store energy by compressing ambient air to high pressures and storing it in tanks or underground caverns. To recover stored energy, the air is then expanded through gas turbines, generating electricity. Traditional diabatic CAES systems reject the heat of compression to the environment, thus losing a significant amount of energy. These systems typically require natural gas firing to heat up the air during discharging. Such systems have been in commercial use for decades, with the Huntorf plant in Germany starting operation in 1978 and the McIntosh plant in the United States in 1991. Jafarizadeh et al. [23] propose several modifications to improve the efficiency of the origin design of the Huntorf plant, including a recuperator, compressor cooling and water and steam injection. Recent research and projects have focused on adiabatic CAES (A-CAES) systems, which include thermal stores to retain some of the heat of compression. This heat is then used to heat up the air before expansion during discharge. This increases the roundtrip efficiency, while eliminating the need for natural gas firing [24]. Another promising novel concept is isothermal CAES. These systems attempt to approximate isothermal pressure changes by using slow compression and expansion, typically performed by a liquid-piston system, thus reducing exergy losses and increasing efficiency [25]. Reaching high power ratings with isothermal CAES is a challenge due to the slow compression and expansion processes required [26], though a prototype rated at 1.5 MW has been built [27].

One of the first A-CAES systems was proposed by Bullough et al. [28] in 2004, with the aim to improve integration of wind energy. The system was envisioned to have 120 to 1,200 MWh of thermal storage capacity operating between 50 and 650 ℃. The authors considered various solid and liquid storage materials, including natural stone beds, concrete walls, and cast-iron slabs, as well as one-tank and two-tank systems with nitrate salt or mineral oil. Grazzini and Milazzo [29] studied the integration of a two-tank liquid thermal energy store (L-TES) into a three-stage compression and expansion CAES. Hartmann et al. [30] present a study of one-, two- and three-stage polytropic A-CAES systems as well as an ideal isentropic system with an unspecified sensible thermal store. Kim et al. [25] performed energy and exergy analyses of a range of CAES systems, including a one-stage A-CAES with a sensible solid TES system and a two-stage A–CAES with a two-tank oil L-TES. Barbour et al. [31] present an extensive analysis of a two-stage A-CAES system with two gravel packed-bed thermal energy stores (PB-TESs). The authors state that steady-state roundtrip efficiencies of over 70% can be reached. The total investment costs are estimated to be about 720 k$ for a 500 kW and 2 MWh system, yielding energy capital costs of 360 $/kWh. Guo et al. [32] investigated a four-stage supercritical CAES system with a two–tank pressurised-water hot L–TES and a cryogenic storage tank. Mousavi et al. [33] present an analysis of a two-stage A–CAES with two phase-change material TES systems and a concrete high-temperature thermal store.

In addition to the large–scale systems for electricity storage, micro CAES for household applications have been proposed [34], which can also integrate renewable generation from solar PV modules [35]. The integration of CAES with other systems, such as a desalination unit [36], a concentrating solar power and desalination system [37], a biomass and geothermal cogeneration system [38], and organic Rankine cycle and absorption chiller [39], different organic Rankine cycle and Kalina cycles [40], and cogeneration systems [41] has also been studied extensively in literature. For more information the reader is referred to review papers by Budt et al. [24] and Olabi et al. [42], while King et al. [43] present an overview of major recent CAES projects and assess the potential for underground storage in India and the United Kingdom.

The studies in literature have shown that CAES can be a promising technology, but systems need to be designed carefully and optimisation can provide significant value. Despite recent advancements in CAES, an extensive analysis and comparison of different CAES configurations optimised for various TES options and materials is missing in literature. Previous studies focus on specific system configurations with predefined TES systems, storage materials and/or component sizes and operating parameters. In this work, a thermodynamic-modelling and component-costing framework is developed to identify optimal A-CAES system designs. The framework is then used to, for the first time, provide a comprehensive comparison of different A–CAES configurations based on PB-TESs and L-TESs, considering different storage materials. In contrast to existing literature, we include the system design, component sizing and operational parameters in a simultaneous optimisation, rather than focussing on pre–designed system layouts or components.

The main goal is to identify optimal A–CAES plant configurations, to provide a comprehensive comparison between different TES systems and storage materials, to investigate economies of scale and to assess the potential of this technology in comparison with other large–scale energy storage technologies. The results are relevant to technology developers, electricity system operators, policymakers, and the scientific community.

2. Methods

Thermo-economic optimisations are performed for different A-CAES system configurations in order to assess the potential of the technology, identify optimal system designs, and evaluate different TES concepts. The thermodynamic component and system models, costing methods and optimisation routine are presented in this section.

2.1. Adiabatic compressed–air energy storage configurations

Fig. 1 shows a schematic overview of the A-CAES configurations investigated in this work. To establish a baseline, systems with a nominal discharge power of 50 MW and charging and discharging durations of 6 h are investigated. This is within the range of most valuable storage durations identified in the literature review and is similar to the related work of Zhao et al. [44]. Further, to assess potential economies of scale as well as trade-offs between energy and power capacity, nominal discharge powers are varied from 10 to 100 MW, while discharge durations of 3 to 9 h are considered.

A two-stage compression-expansion process is assumed, with either one or two PB-TESs or L–TESs. Ambient air, which is assumed to be dry air at 15 ℃ and 1 bar, is compressed in the first compressor. Some of the

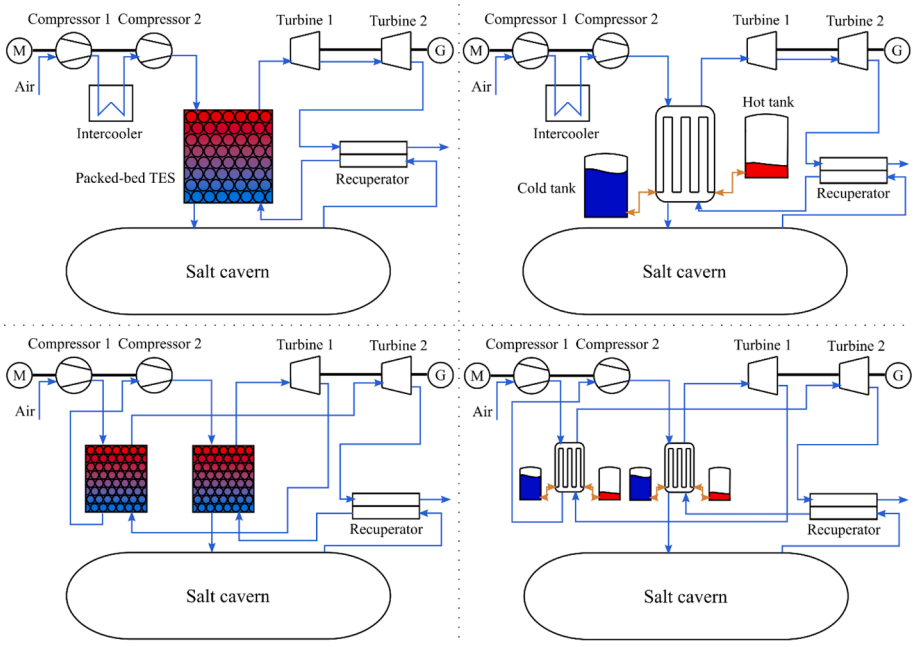

Fig. 1. A-CAES configurations investigated in this work: intercooler and PB-TES (top left); intercooler and L-TES (top right); two PB-TESs (bottom left); and two L-TESs (bottom right). In all cases, a two-stage compression is assumed, as well as the presence of a recuperator, which recovers heat from the exhaust stream to pre-heat the cold air.

heat of the first compression is then rejected in a finned-tube intercooler or stored in the first thermal store in order to reduce second-stage compression work. The second compressor then compresses the air to its final pressure. The hot, high-pressure air then passes through a PB-TES or a shell-and-tube heat exchanger (ST-HEX) connected to an L–TES, before being stored in a salt cavern. The temperature of the air in the cavern is assumed to be constant at 15 ℃. The compressors are assumed to have fixed compression ratios, meaning that they always generate the maximum pressure regardless of the current pressure of the air cavern. This results in exergy destruction and efficiency losses due to throttling but is more representative of the limited flexibility that most compressors have in practice.

For discharging, the air from the cavern is heated up in the packed bed or ST-HEX and then expanded through the turbines, driving a generator to generate electricity. In the system configurations with two thermal stores, the air is reheated after the first expansion using heat from the second thermal store. To improve the efficiency, the systems also include a recuperator in which excess heat is transferred from the exhaust air to pre-heat the high-pressure air leaving the cavern. The recuperator is assumed to be an ST-HEX with the high-pressure air flowing on the tube-side and the low-pressure air on the shell-side. Like the compressors, the turbines are assumed to have fixed expansion ratios, meaning that the air from the cavern is always throttled to the minimum cavern operating pressure, again resulting in exergy losses and a reduction of efficiency.

The availability of a salt cavern with a total volume of up to $1{\cdot}10^6$ m^3 to store the compressed air is assumed. This is about three times as large as the one used for the Huntorf diabatic CAES plant and twice as large as the McIntosh plant cavern. Salt caverns and other underground formations up to that size are available in many regions worldwide [45]. The maximum cavern pressure operating range is assumed to be 46 to 72 bar, in line with the Huntorf plant [24].

2.2. Thermodynamic component models

The main components of the considered A-CAES configurations are compressors and turbines (assumed to be turbomachines), intercoolers (assumed to be finned-tube air coolers), PB-TESs and L-TESs, liquid storage heat exchangers (assumed to be ST–HEX), the recuperator (assumed to be an ST–HEX) and the salt cavern as an isochoric air-storage reservoir. The thermodynamic models of these components and the whole system are presented in this section.

The working fluid is assumed to be dry air. All its properties are calculated from the CoolProp library [46], using the low-level interface to achieve sufficient calculation speed.

The compressors and turbines are modelled using the polytropic efficiency, η_p, as a performance indicator, which compares the actual process to a theoretical, infinitesimally small and reversible compression or expansion process. The expressions for the compressor and turbine temperature and pressure ratios are:

$$\frac{T_{\mathrm{comp,out}}}{T_{\mathrm{comp,in}}} = \left(\frac{p_{\mathrm{comp,out}}}{p_{\mathrm{comp,in}}}\right)^{\frac{\gamma-1}{\gamma}\frac{1}{\eta_{\mathrm{p,comp}}}}; \tag{1}$$

$$\frac{T_{\mathrm{turb,out}}}{T_{\mathrm{turb,in}}} = \left(\frac{p_{\mathrm{turb,out}}}{p_{\mathrm{turb,in}}}\right)^{\frac{\gamma-1}{\gamma}\eta_{\mathrm{p,turb}}}, \tag{2}$$

with T and p being the temperatures and pressures at the compressor (comp) and turbine (turb) inlets (in) and outlets (out), respectively, and γ being the ratio of isobaric to isochoric specific heat capacity c_p/c_v. The polytropic efficiencies are estimated based on the pressure ratio using the correlations of Wilson [47], presented by Wang et al. [48]:

$$\eta_{\mathrm{p,comp}} = 0.91 - \frac{\left(\frac{p_{\mathrm{comp,out}}}{p_{\mathrm{comp,in}}}\right) - 1}{300}; \tag{3}$$

$$\eta_{\mathrm{p,turb}} = 0.90 - \frac{\left(\frac{p_{\mathrm{turb,in}}}{p_{\mathrm{turb,out}}}\right) - 1}{250}. \tag{4}$$

The intercoolers, if present, are assumed to be finned-tube air coolers. As shown in Fig. 1, intercoolers are present in the first two configurations with only one TES each. They cool down the air between the two compression stages, leading to heat losses to the environment. The intercoolers are modelled using the methodology presented by Hewitt [49], assuming a triangular configuration of finned-tube bundles. The ideal Nusselt number Nu and heat transfer coefficient α are

calculated from the Kaunas correlation [49], based on the Reynolds and Prandtl numbers, Re and Pr, as well as geometric parameters a, b, s, d, and h:

$$\mathrm{Nu} = \begin{cases} 0.19\left(\frac{a}{b}\right)^{0.2}\left(\frac{s}{d}\right)^{0.18}\left(\frac{h}{d}\right)^{-0.14} Re^{0.8}Pr^{0.33} \text{ if } Re < 2{\cdot}10^4 \\ 0.05\left(\frac{a}{b}\right)^{0.2}\left(\frac{s}{d}\right)^{0.18}\left(\frac{h}{d}\right)^{-0.14} Re^{0.8}Pr^{0.36} \text{ if } Re < 2{\cdot}10^5 \\ 0.008\left(\frac{a}{b}\right)^{0.2}\left(\frac{s}{d}\right)^{0.18}\left(\frac{h}{d}\right)^{-0.14} Re^{0.95}Pr^{0.36} \text{ if } Re > 2{\cdot}10^5 \end{cases} \quad (5)$$

$$\alpha = \mathrm{Nu}\frac{\lambda}{d}. \quad (6)$$

The Reynolds number is hereby calculated based on the maximum fluid velocity v_m, which occurs at the minimum free cross section of the finned-tube bank, the tube diameter at the fin base d, and the fluid density ρ and viscosity ψ [49]:

$$\mathrm{Re} = \frac{\rho v_m d}{\psi}. \quad (7)$$

The ideal heat transfer coefficient is then corrected with the fin efficiency ϕ, which is calculated assuming constant fin thickness and neglecting fouling as:

$$\phi = \frac{\tanh(m_e h_e)}{m_e h_e}(1 - 0.058(m_e h_e)), \quad (8)$$

with geometric parameters m_e and h_e. Finally, the effective heat transfer coefficient α_e is calculated using the total area A_t, the fin area A_f and the unfinned area A_r:

$$\alpha_e = \alpha\frac{\phi A_f + A_r}{A_t}. \quad (9)$$

PB-TESs are modelled using a discretised, dynamic model based on the semi-analytical approach developed by White [50]. Sciacovelli et al. [51] have demonstrated the importance of having a dynamic energy storage model in any assessment of A–CAES systems. Assuming non-compressible air flow through the (cylindrical) bed, and neglecting axial and radial heat conduction as well as temperature gradients within the pebbles (an assumption that holds for small Biot numbers), the energy conservation equations are:

$$(1-\epsilon)\rho_s c_{p,s}\frac{\partial T_s}{\partial t} = \alpha_{gs}(T_g - T_s); \text{(solid phase)} \quad (10)$$

$$\epsilon\rho_g c_{p,g}\frac{\partial T_g}{\partial t} + \rho_g c_{p,g} v_g \nabla T_g = \alpha_{gs}(T_s - T_g), \text{(gas phase)} \quad (11)$$

with ρ_s and ρ_g being the solid and gas densities and ϵ the void fraction of the packed bed. The superficial fluid velocity is denoted by v_g, which is defined as the overall gas volume flowrate divided by the cross-sectional area of the packed bed. The volumetric heat transfer coefficient, α_{gs}, is calculated from the correlation proposed by Löf and Hawley [52]:

$$\alpha_{gs} = 650\left(\frac{\dot{m}_g}{AD_p}\right)^{0.7}, \quad (12)$$

where $\dot{m}_g$ denotes the mass flowrate of the gas, A the cross-sectional area of the packed bed and D_p the pebble diameter [53]. The correlation was developed from experimental data on heat transfer coefficients in gravel-packed beds. The factor of 650 stems from the conversion of the original correlation from imperial to SI units. The semi-analytical solution approach involves the analytical integration of the energy conservation equations between two nodes, treating the temperature as constant. With this method, larger time steps can be taken compared to a classic finite-difference method [50]. Convergence studies have been performed to identify appropriate time steps and length increments for the discretisation for the packed-bed sizes considered in this study. A time step of $\Delta t = 100$ s and a length increment of $\Delta x = 0.025$ m were chosen.

The L-TESs are modelled as two well-mixed tanks, a hot store and a cold store, between which the heat storage fluid, also acting as heat transfer fluid, is pumped. An ST–HEX is installed between the tanks, it acts as interface to the CAES cycle. During charging, fluid is pumped from the cold to the hot store, gaining heat in the ST-HEX and cooling down the compressed air in the process. For discharging, the fluid flow is reversed, so that fluid from the hot store can provide heat to the compressed air prior to the expansion. The storage fluid mass flowrate is assumed to be constant throughout the process. It is optimised in order to achieve the ideal storage temperatures.

Different storage materials are considered for both the PB-TESs and the L-TESs. A summary of the main characteristics of the materials is presented in Table 1 and Table 2. Note that the values shown in the Table 2 are indicative only, as they depend on the fluid temperature. In the model, the properties of L-TES materials are calculated based on the temperature from the correlations used by Zhao et al. [44]. It should also be noted that energy costs for producing the materials, as well as transport costs, have recently increased significantly. Therefore, the values reported here, taken from literature sources, may not correspond to latest market prices.

All ST-HEXs are modelled using a dimensionless ε-NTU method, using the Bell-Delaware method described by Hewitt [49] to calculate the overall heat transfer coefficient. The heat exchanger effectiveness ε represents the ratio of actual to theoretical maximum heat transfer rate.

For ST-HEXs, the effectiveness can be estimated as:

$$\varepsilon = \frac{1 - \exp(-\mathrm{NTU}(1 - C_R))}{1 - C_R\exp(-\mathrm{NTU}(1 - C_R))}. \quad (13)$$

Here, C_R is the minimum to maximum heat capacity flow ratio and NTU the number of transfer units:

$$\mathrm{NTU} = \frac{\alpha A}{(\dot{m}c_p)_{min}}, \quad (14)$$

where A denotes the effective heat transfer area and α the overall heat transfer coefficient, which is calculated according to the approximate method of Hewitt [49] and neglecting fouling:

$$\alpha = \frac{1}{\frac{1}{\alpha_{ts}}\frac{d_{out}}{d_{in}} + \frac{\delta_w}{\lambda_w}\frac{d_{out}}{d_m} + \frac{1}{\alpha_{ss}}}, \quad (15)$$

with α_{ts} and α_{ss} the tube-side and shell-side heat transfer coefficients, δ_w and λ_w the wall thickness and thermal conductivity, and d_{in}, d_m and d_{out} the inner, mean, and outer tube diameters.

The tube–side heat transfer coefficient is calculated from the Petukhov-Kirillov correlation [54] for the Nusselt number, Nu, based on the Reynolds and Prandtl numbers, Re and Pr:

Table 1
Density, specific heat capacity, thermal conductivity and cost of PB-TES materials considered in this study. Material selection and data are based on Zhao et al. [44].

Name	Density [kg/m^3]	Specific heat capacity [J/kg/K]	Thermal conductivity [W/m/K]	Cost [$/kg]
Magnetite	5,080	851	4.91	0.50
Quartzite	2,500	830	3.16	0.04
Alumina	3,990	1,170	11.1	1.50
Titanium oxide	4,230	692	8.40	1.70
Hematite	5,240	628	12.6	0.50
Basalt	2,640	1,230	1.50	0.12

Table 2
Temperature range, density, specific heat capacity, thermal conductivity, viscosity and cost of L-TES materials considered in this study. Material selection and data are based on Zhao et al. [44]. The values for density, specific heat capacity, thermal conductivity and viscosity shown in the table were calculated at the average of the temperature range. In the model, all temperature-dependant values are calculated for the appropriate temperature.

Name	Min. temp. [°C]	Max. temp. [°C]	Density [kg/m^3]	Specific heat capacity [J/kg/K]	Thermal conductivity [W/m/K]	Viscosity [mPa.s]	Cost [$/kg]
HITEC	142	535	1,640	1,560	0.382	2.60	0.93
HITEC XL	130	550	1,960	1,430	0.519	4.19	1.43
Solar salt	260	600	1,820	1,520	0.525	1.57	0.50
Therminol 66	−9	343	910	2,070	0.109	1.20	1.00
Therminol VP-1	12	400	910	2,070	0.113	0.37	3.96
Rapeseed oil	7	250	840	2,380	0.195	7.59	0.80

$$\mathrm{Nu} = \frac{(f/8)\mathrm{Re}\,\mathrm{Pr}}{12.7^{*}(f/8)^{0.5}(\mathrm{Pr}^{2/3}-1)+1.07}; \qquad f = \frac{1}{(0.79\ln(\mathrm{Re})-1.64)^{2}}. \tag{16}$$

The heat transfer coefficient is calculated for an ideal tube bank as in Hewitt [49]:

$$\alpha_i = \frac{j_i c_p \dot{m}}{\mathrm{Pr}^{2/3}}\Phi^{r}; \tag{17}$$

$$j_i = a_1\left(\frac{1.33}{L_{tp}/d_m}\right)^{\frac{a_3}{1+0.14\mathrm{Re}^{a_4}}}\mathrm{Re}^{a_2}, \tag{18}$$

with ϕ^r denoting the viscosity correction (neglected in this work) and L_{tp} the distance between tubes. The coefficients a_1 to a_4 are determined for different flow regimes based on Re. The shell-side heat transfer coefficient is then calculated using correction factors, J:

$$\alpha_{ss} = \alpha_i(J_c J_l J_b J_s J_r). \tag{19}$$

Average correction factors mentioned by Hewitt [49] are used, and design recommendations from the same book are followed to determine appropriate dimensions.

With these component models, the overall operation of the CAES can be modelled and key performance indicators can be calculated. The roundtrip efficiency η is defined as ratio of generated electricity from discharging to consumed electricity for charging:

$$\eta = \frac{\sum_{\mathrm{discharging}}\left(\dot{W}_{\mathrm{el,turb,1}} + \dot{W}_{\mathrm{el,turb,2}}\right)}{\sum_{\mathrm{charging}}\left(\dot{W}_{\mathrm{el,comp,1}} + \dot{W}_{\mathrm{el,comp,2}}\right)}. \tag{20}$$

The main economic indicators are the energy capital costs, C_{EC}, and the power capital costs, C_{PC}. The former is defined as ratio of total capital costs, C_t, to total recovered energy:

$$C_{EC} = \frac{C_t}{\sum_{discharging}\left(\dot{W}_{\mathrm{el,turb,1}} + \dot{W}_{\mathrm{el,turb,2}}\right)}. \tag{21}$$

The power capital costs are defined as ratio of total capital cost to nominal discharge power:

$$C_{PC} = \frac{C_t}{\dot{W}_{\mathrm{el,turb,1}} + \dot{W}_{\mathrm{el,turb,2}}}. \tag{22}$$

The A-CAES system is modelled over 10 charging and discharging cycles to reach steady-state conditions and eliminate the effect of assumptions on the initial state. During discharging, if the thermal stores are empty, the turbines are bypassed and the air is expanded via an isenthalpic throttle valve, generating no power. This is achieved by enforcing a minimum turbine outlet temperature of 0 °C.

2.3. Costing methods

To calculate the economic performance indicators, it is necessary to estimate the investment costs of different system designs. This is achieved by calculating the approximate costs of each individual component based on specific size parameters, such as the nominal power of turbomachinery or heat exchanger areas. The total investment cost is then the sum of all component costs and the storage material cost, taken from Table 1 and Table 2.

Since such component cost correlations are associated with significant uncertainties (see also Table 3) and the underlying data is usually not available, correlations from multiple sources are used for each component. In the calculation of energy and power capital cost, the values from the different sources are then averaged to achieve a more robust representation of total capital costs.

Cost correlations for turbomachinery at the sizes required here are scarce. Rosner et al. [55] developed a correlation for large-scale gas turbines, which is used here to get one cost data point. The same correlation is also used for the compressors, assuming that costs are similar to turbines. Additionally, the correlations of Ulrich [56], Turton [57], Seider [58] and Morandin [59] are used, assuming axial gas turbines made from carbon steel. It should be noted however that the values from the first three correlations must be extrapolated, and the valid range of the last one is unknown. Therefore, values should be treated with care.

The intercoolers are costed as air coolers, using the correlations proposed by Turton [57] and Couper [60]. The cost correlations of Ulrich [56], Turton [57], Seider [58] and Couper [60] are considered for the ST-HEXs, again assuming carbon steel construction where relevant, as well as floating-head design where available. The same four sources, as well as Morandin [59], also provide correlations for storage tanks and pumps, which are used to estimate the costs of the L-TESs. The PB-TESs must withstand the high pressure of the compressed air. Therefore, they are costed as pressure vessels, using the correlations of Ulrich [56], Turton [57], Seider [58], Morandin [59] and Couper [60] for horizontal pressure vessels made from carbon steel. The storage materials are costed based on their weight according to Table 1 and Table 2. The Chemical Engineering Plant Costing Index (CEPCI) [61] is used to account for inflation. All costs are adjusted to December 2021 US dollars ($).

Table 3 shows the component costs predicted from the different cost correlations for two reference configurations (see also Section 3.1). The correlation of Ulrich [56] consistently predicts at least four times higher compressor costs than all other correlations. It is therefore deemed to be an outlier and excluded from the investment cost averaging. Likewise, the correlation of Turton [57] for pressure vessels is excluded, as it predicts costs at least seven times higher than all other correlations. Additionally, the correlation of Morandin [59] for PB-TESs is excluded, as it predicts costs more than four times lower than all other correlations, and it is only valid for pressures below 10 bar.

2.4. Optimisation

A numerical optimisation algorithm is used to identify optimal system designs. Objectives are set to either maximise the roundtrip efficiency for a pure thermodynamic optimisation or to minimise the energy capital cost for a thermo-economic optimisation.

Table 3
Component costs of the cost-optimal systems with one PB-TES filled with Magnetite and one L-TES with HITEC (see also Section 3.1) calculated from the different costing correlations considered in this study.

Component	Rosner [55]	Ulrich [56]	Turton [57]	Seider [58]	Morandin [59]	Couper [60]
			One PB-TES with Magnetite			
Compressor 1	17 M$	209 M$	20 M$	15 M$	9 M$	–
Compressor 2	17 M$	266 M$	22 M$	18 M$	11 M$	–
Turbine	20 M$	11 M$	2 M$	8 M$	26 M$	–
PB-TES	–	3 M$	82 M$	2 M$	1 M$	10 M$
Recuperator	–	0 M$	0 M$	0 M$	–	0 M$
			One L-TES with HITEC			
Compressor 1	17 M$	110 M$	15 M$	10 M$	6 M$	–
Compressor 2	31 M$	560 M$	29 M$	29 M$	17 M$	–
Turbine	24 M$	11 M$	2 M$	8 M$	27 M$	–
L-TES	–	1 M$	3 M$	3 M$	2 M$	1 M$
ST-HEX	–	1 M$	3 M$	2 M$	–	5 M$
Recuperator	–	1 M$	4 M$	1 M$	–	3 M$

Since the objective function is computationally expensive to calculate (as the system is simulated over 10 charging and discharging cycles) and derivatives are not readily available, the surrogate optimisation algorithm in MATLAB R2022a [62] is used to solve the problem. The solver uses a derivative–free algorithm: it chooses a number of trial points at which the (computationally expensive) objective function is evaluated, and then creates a (computationally cheap) surrogate model by interpolation through the trial points. Then, good candidate points (i.e., points with a low objective function value) are identified from the surrogate model. The expensive objective function is then evaluated at these candidate points and the surrogate model is updated. Since the solver uses a derivative–free algorithm, it cannot provide any optimality indicators. Therefore, a maximum number of 5,000 expensive objective function evaluations is used as termination criterion. Trials showed that this led to reliable identification of near–optimal solutions. The solution is then refined using the interior-point optimisation algorithm implemented in the *fmincon* function in MATLAB [63], using the solution of the surrogate optimisation as starting point for the optimisation.

The decision variables for the optimisation are the:

- pressure ratio of the first compressor (the pressure ratio of the other is then given by the overall pressure ratio);
- pressure ratio of the first turbine (the pressure ratio of the other is then given by the overall pressure ratio);
- air mass flowrate;
- size of the intercooler, if present;
- size of the recuperator;
- volume of the PB-TESs, if present;
- design of the L-TESs, if present, including:
  - o volume of the storage tanks;
  - o size of the heat exchanger;
  - o mass flowrate of the storage medium.

Table 4 shows an overview of decision variables with lower and upper bounds. Tighter bounds make it easier for the optimiser to find the optimal solution, as the search space is reduced, but care must be taken to not exclude feasible solutions that might be optimal.

Constraints, together with the bounds on decision variables, ensure the feasibility of the optimal solution. In this study, constraints are used to limit the thermal store temperatures. For L-TESs, the storage temperatures are limited to the maximum working temperature of the storage material, as shown in Table 2. The temperatures of the PB-TESs are not limited by the storage material, but by the pressure vessel. The upper limit is set to 400 ℃, as higher temperatures would require different materials and significant engineering work [24]. The maximum allowable temperature in the ST-HEXs is set to 600 ℃ [64].

3. Results and discussion

Results from thermo-economic optimisations of the A-CAES configurations shown in Fig. 1, with the thermal storage materials listed in Table 1 and Table 2, at different scales are presented in this section. First, to establish a benchmark, a system with a single PB-TES with Magnetite and one with a single L-TES with HITEC salt with a nominal discharge power rating of 50 MW and charging/discharging durations of 6 h (each) are investigated. Then, systems with different storage materials and systems with a second store are compared. Finally, the effect of the scale of the CAES is investigated by comparing performance across different nominal discharge power ratings and charging/discharging durations.

3.1. Systems with one packed–bed thermal energy store with Magnetite and one liquid thermal energy store with HITEC

Table 5 shows a summary of key decision variables and performance indicators of the two benchmark configurations optimised for maximum roundtrip efficiency or minimum energy capital costs. The systems optimised for maximum efficiency have larger thermal stores and larger heat exchangers, allowing them to achieve higher efficiencies. The large thermal stores guarantee that no heat is wasted. The larger heat exchangers result in smaller temperature differences in the heat exchanger and therefore higher storage temperatures, higher turbine inlet temperatures and ultimately higher efficiencies. However, these designs result in significantly higher total capital costs and therefore higher energy and power capital costs.

The difference in energy capital costs between the highest-efficiency and least-cost systems with one PB–TES are over 100 $/kWh while the difference in efficiency is 11% points. In terms of power capital costs, the

Table 4
Decision variables with lower and upper bounds for the optimisation. Component sizing and operational parameters are optimised simultaneously.

Name	Comp. 1 pressure ratio [-]	Turb. 1 pressure ratio [-]	Air mass flowrate [kg/s]	Inter-cooler size [m^2]	Recu-perator size [m^2]	Packed-bed volume [m^3]	Liquid tank volume [m^3]	L-TES HEX size [m^2]	L-TES flowrate [kg/s]
Lower bound	1	1	10	0	0	100	100	100	20
Upper bound	46	46	500	10,000	5,000	10,000	20,000	10,000	1,000

Table 5
Key characteristics of the benchmark configurations for a discharge power of 50 MW and a discharge duration of 6 h, optimised for maximum efficiency or minimum energy capital cost.

Storage	Material	Objective	Storage volume [m^3]	ST-HEX size [m^2]	Roundtrip efficiency [-]	Power capital cost [$/kW]	Energy capital cost [$/kWh]
1PB-TES	Magnetite	Efficiency	7,000	–	58%	1,830	260
1PB-TES	Magnetite	Cost	1,770	–	47%	1,080	150
1 L-TES	HITEC	Efficiency	19,500	3,900	39%	2,030	290
1 L-TES	HITEC	Cost	5,810	2,820	33%	1,390	200

highest-efficiency system is 750 $/kW more expensive. The results are similar for the system with one L-TES, where the most efficient system in 6% points more efficient, but 95 $/kWh and 640 $/kW more expensive.

It should be noted that the optimal trade-off between efficiency and cost cannot be determined from the analysis carried out here, as it depends on many factors, including the cost of electricity used for charging. Economic indicators that account for these costs, such as levelised-cost-of-storage (LCOS), can be used to investigate this further, and whole-energy system modelling can be useful in determining if efficiency or cost should be prioritised.

The efficiencies of the benchmark systems with L-TES are significantly lower compared to the systems with PB–TES. This can be explained by the worse heat transfer in the ST–HEXs compared to the direct heat transfer in PB-TESs, which leads to lower storage and turbine inlet temperatures. At the same time, the energy and power capital costs of the systems with L-TES are higher. The cost–optimal system with PB-TES is 42 $/kWh and 310 $/kW cheaper compared to the system with L–TES while also being 14% points more efficient. The higher efficiency would favour the system with PB-TES even more in terms of LCOS. However, it is important to note that the capital costs are uncertain, as shown in Table 3.

The energy and power capital cost values shown in Table 5 were calculated from the average of the component costs obtained from the considered cost correlations. These averaged cost values are also used in the objective function of the optimisation. Depending on the component cost correlations used, the energy capital costs of the cost-optimal system with PB–TES vary from 80 to 230 $/kWh, while for the cost-optimal system with L–TES they vary from 110 to 270 $/kWh. The variation in power capital costs is 560 to 1,640 $/kW and 780 to 1,910 $/kW, respectively.

Fig. 2 shows a cost breakdown by component of the cost-optimal designs of the benchmark configurations. The investment costs of both systems are dominated by the turbomachines, which account for 84% and 76% of the total costs, respectively. The pressure vessel accounts for 9% of the costs of the system with PB–TES, while the storage material accounts for 6%. For the system with L-TES, the storage material costs are more significant, accounting for 13% of the total investment costs. Heat exchanger and liquid storage tank are responsible for 4% and 3% of the total investment costs, respectively.

Fig. 2 is a good indicator of effective levers to reduce costs. Both systems would benefit significantly from reduced turbomachinery costs. For the system with PB-TES the pressure vessel should also be prioritised for further cost-reduction efforts, while for the system with L-TES reducing the storage material costs can have a significant impact on total costs.

3.2. *Different storage materials and systems with two thermal stores*

Following the investigation of A-CAES systems with a single thermal store and one specific storage material, the influence of different storage materials and of adding a second thermal store is explored in this section. Fig. 3 shows an overview of energy capital costs and roundtrip efficiencies of different systems optimised for minimum energy capital costs, with error bars representing the range of capital costs calculated from different correlations. Fig. 4 shows the corresponding power capital costs, again with error bars representing different correlations.

The first thing to note is that the uncertainties in capital costs are higher than the differences in performance between the different storage

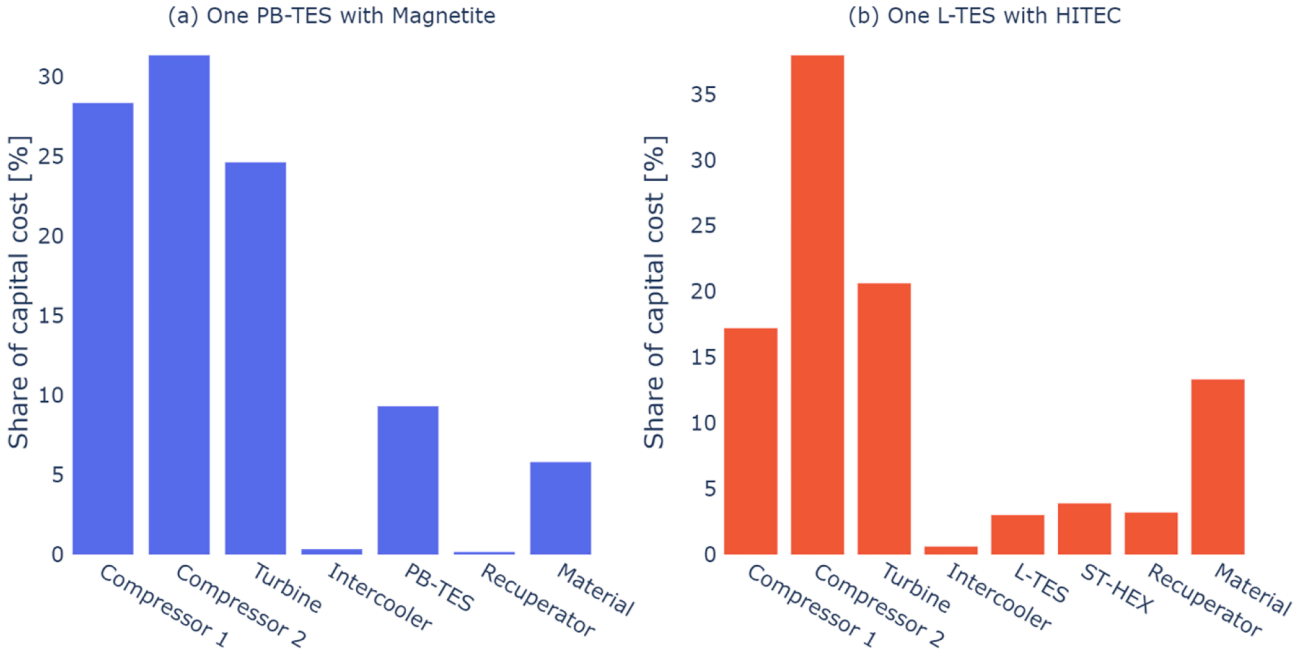

Fig. 2. Breakdown of investment costs by component of: (a) the cost-optimal system with one PB–TES filled with Magnetite; and (b) the cost-optimal system with one L-TES with HITEC. The bars show the relative importance of different components for the investment costs.

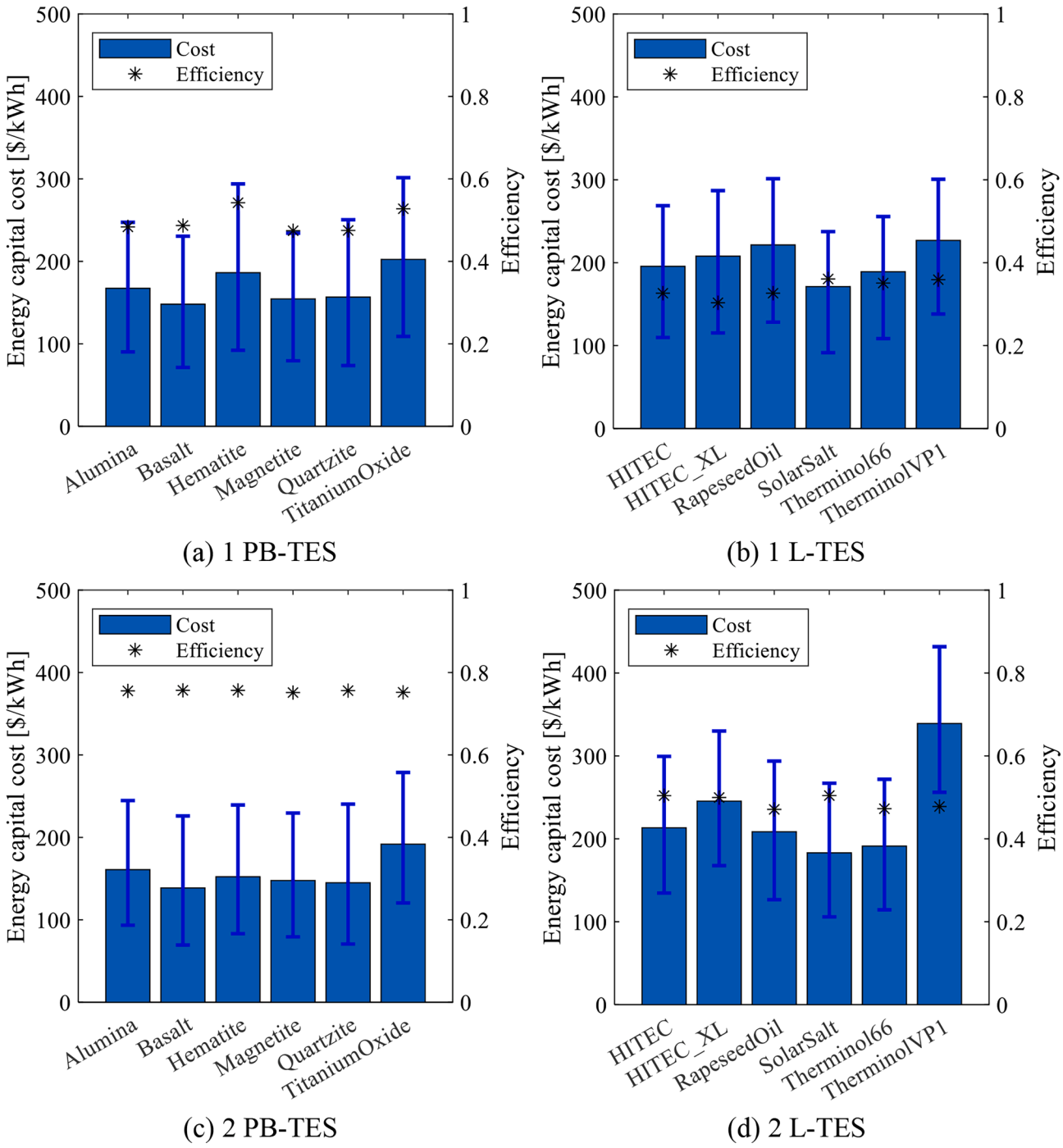

Fig. 3. Energy capital cost and roundtrip efficiency of the cost-optimal systems with: (a) one PB-TES; (b) one L-TES; (c) two PB-TESs; and (d) two L-TESs, using different thermal storage materials. The bars show the energy capital cost (left *y*-axis), with error bars showing the energy capital cost ranges associated with the use of different component costing correlations. The markers show the roundtrip efficiency (right *y*-axis).

materials. However, since the cost uncertainties are due to different component cost correlations, they are largely systematic uncertainties. This means that the costs of systems with different materials are affected in a similar way (i.e., the use of different correlations would shift all costs in the same direction).

Basalt is the best-performing solid storage material in terms of energy capital costs. The optimal system with 1 PB–TES reaches energy capital costs of 150 $/kWh. Basalt combines a high specific heat capacity with low material costs. Magnetite, Quartzite and Alumina reach marginally higher minimum energy capital costs at 150 $/kWh, 160 $/kWh and 170 $/kWh, respectively. Titanium oxide performs worst due to high material costs and a low specific heat capacity. The energy capital costs of the cost-optimal system are 54 $/kWh or 36% higher than those of the best-performing material (Basalt). The cost-optimal systems with 1 PB-TES achieve roundtrip efficiencies of 47 to 54%, while power capital costs are in the range of 1,050 to 1,440 $/kW.

The difference in performance between different storage materials is similar for systems with 1 L–TES compared to systems with 1 PB–TES. Solar salt performs best, reaching energy capital costs of 170 $/kWh. It combines the highest temperature limit with a high heat capacity and low material costs. TherminolVP1 on the other hand shows the highest optimal energy capital costs at 230 $/kWh, 33% higher compared to

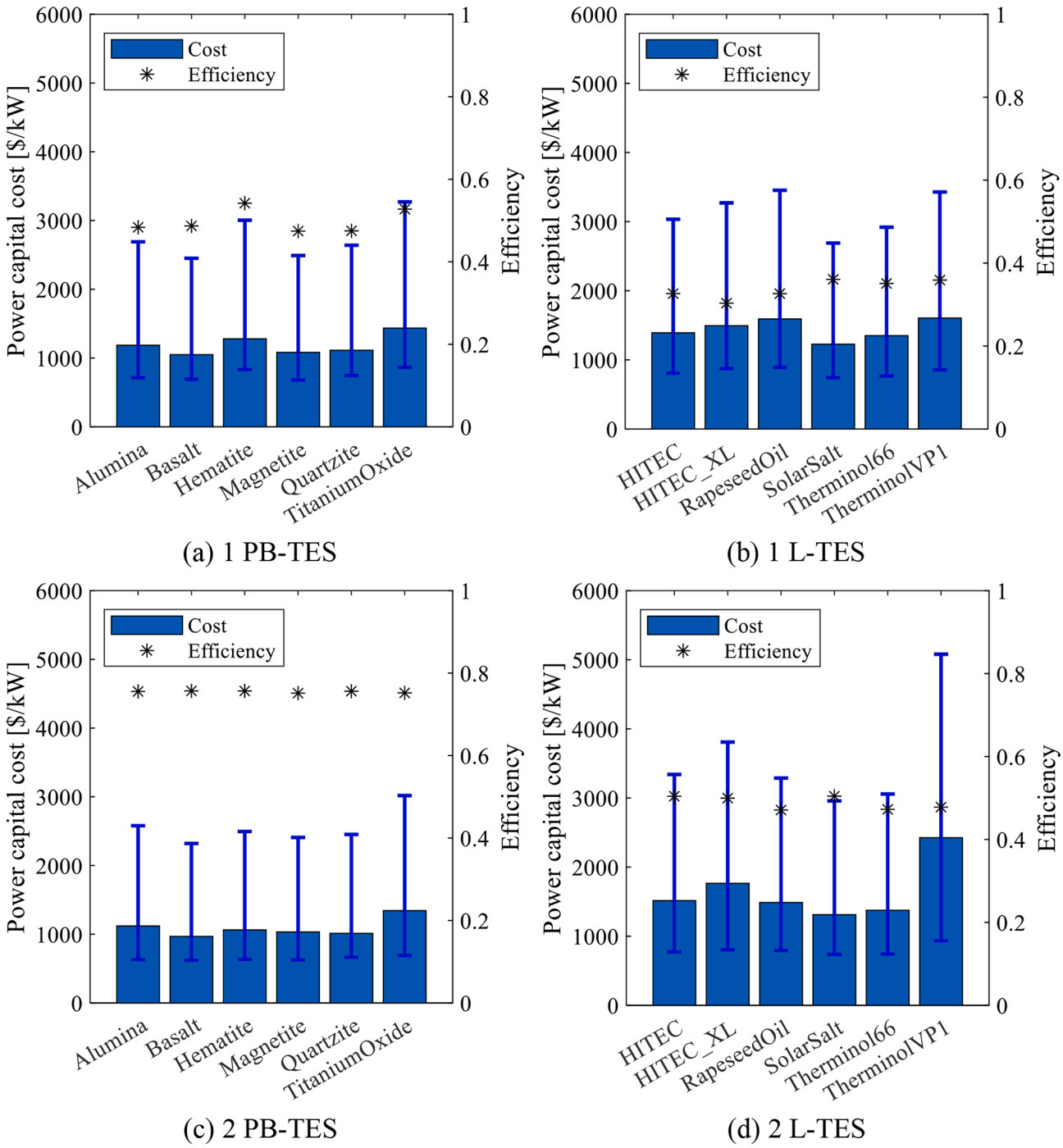

Fig. 4. Power capital cost and roundtrip efficiency of the cost-optimal systems with: (a) one PB-TES; (b) one L-TES; (c) two PB-TESs; and (d) two L-TESs, using different thermal storage materials. The bars show the power capital cost (left y-axis), with error bars showing the power capital cost ranges associated with the use of different component costing correlations. The markers show the roundtrip efficiency (right y-axis).

solar salt. It has the highest material cost and a relatively low upper temperature limit. Rapeseed oil also performs relatively poorly at 220 $/kWh due to having the lowest upper temperature limit. Being able to reach higher temperatures favours both high efficiencies and low specific costs. As already shown in the previous section, the efficiencies of all cost–optimal systems with 1 L-TES are notably lower than these of systems with 1 PB–TES, with values between 30 and 36%. The power capital costs of systems with 1 L-TES on the other hand are higher compared to systems with 1 PB-TES. They range from 1,230 to 1,600 $/kW.

Adding a second PB-TES to the system improves both costs and roundtrip efficiency regardless of the storage material. On average, the optimal energy capital costs improve by 13 $/kWh or 8%, while for Hematite the improvement is as large as 34 $/kWh. The lowest energy capital costs of 140 $/kWh are again reached with Basalt as storage material. The corresponding power capital costs are 970 $/kW. The improvement in roundtrip efficiency is even higher. On average, the systems with 2 PB–TES are 26% points more efficient, so that the roundtrip efficiencies of all cost-optimal systems with 2 PB–TES are between 75 and 76%.

The effect of including a second L-TES instead of an intercooler is less uniform. While for Rapeseed oil the optimal energy capital costs

decrease by 13 $/kWh, they increase for all other liquid storage materials. Due to the low upper temperature limit, Rapeseed oil benefits most from the added thermal store, while for the other materials the effect of added costs due to the additional heat exchanger and storage tanks dominate. The roundtrip efficiencies on the other hand increase for all materials when adding a second L–TES, on average by 15% points. The cost-optimal systems with 2 L-TES reach roundtrip efficiencies of 47 to 50%, while power capital costs are in the range of 1,310 to 2,420 $/kW.

It should be noted that, since the systems shown in Fig. 3 are optimised for least cost rather than maximum efficiency, the efficiencies shown in the plots do not represent the maximum achievable efficiencies for these systems. The identified energy and power capital costs are well within the ranges identified in the review paper of Olympios et al. [18].

3.3. Different nominal discharge powers and charging/discharging durations

To investigate the economies of scale of A-CAES systems, the thermo-economic optimisation is performed for nominal discharge powers of 10, 50 and 100 MW and charging/discharging durations of 3, 6 and 9 h. The resulting optimal energy and power capital costs considering all system configurations and solid and liquid storage materials are shown in Fig. 5. As previously, the systems are optimised for minimum energy capital costs.

The cost-optimal configuration in each case is the system with 2 PB–TESs using Basalt as storage material. This highlights that this configuration shows the best performance over a wide range of operating conditions and is therefore an attractive candidate for further industrial development. However, as previously shown, other solid storage material can reach only slightly higher energy capital costs and should therefore also warrant consideration.

Fig. 5 shows that the specific costs of A-CAES systems are strongly influenced by economies of scale. The energy capital costs decrease significantly with both, increasing nominal discharge power and increasing charging/discharging durations. Both parameters affect the total amount of energy stored. The results show initially strongly decreasing energy capital costs with increasing system size, but also diminishing returns. While at 10 MW and 3 h the minimum energy capital costs are 410 $/kWh, they decrease to 140 $/kWh at 50 MW and 6 h, until ultimately reaching 80 $/kWh at 100 MW and 9 h.

The power capital costs on the other hand show a strong dependence on the nominal discharge power, while the charging/discharging durations only plays a secondary role. Longer charging/discharging durations require larger stores, while not impacting the nominal power, thus the power capital costs increase. However, since the stores only account for a fraction of total capital costs, as shown in Fig. 2, the effect is not as strong the effect of increasing the nominal discharge power. The highest power capital costs of 2,510 $/kW are found at 10 MW and 9 h, while the lowest ones of 690 $/kW are reached at 100 MW and 3 h.

A-CAES systems with L-TESs have higher energy and power capital costs over the entire range of nominal discharge powers and charging/discharging durations considered in this study. The optimal energy capital costs and corresponding power capital costs of the cost-optimal configurations with L-TESs are shown in Fig. 6.

The A–CAES systems with L–TESs show similar economy of scale trends as the systems with PB–TESs. The highest optimal energy capital costs of 510 $/kWh are found at 10 MW and 3 h, while the value decreases to 170 $/kWh at 50 MW and 6 h, and to 90 $/kWh at 100 MW and 9 h. The highest power capital costs of 3,760 $/kW are found at 10 MW and 9 h, while the lowest value of 860 $/kW is reached at 100 MW and 3 h.

The difference in optimal energy capital costs between systems with L–TESs and systems with PB–TESs is 105 $/kW at 10 MW and 3 h, while it decreases to 10 $/kW at 100 MW and 9 h. This corresponds to a relative cost difference of 26% and 11%, respectively. These results suggests that systems with L-TESs become more and more competitive as the system size increases.

3.4. Comparison to other electrical energy storage technologies

Results from this work show that A-CAES systems with a discharge power of 50 MW and a charging/discharging duration of 6 h can achieve an energy capital cost of 140 $/kWh and a power capital cost of 970 $/kWh at a roundtrip efficiency of 76%. Table 6 shows how these values

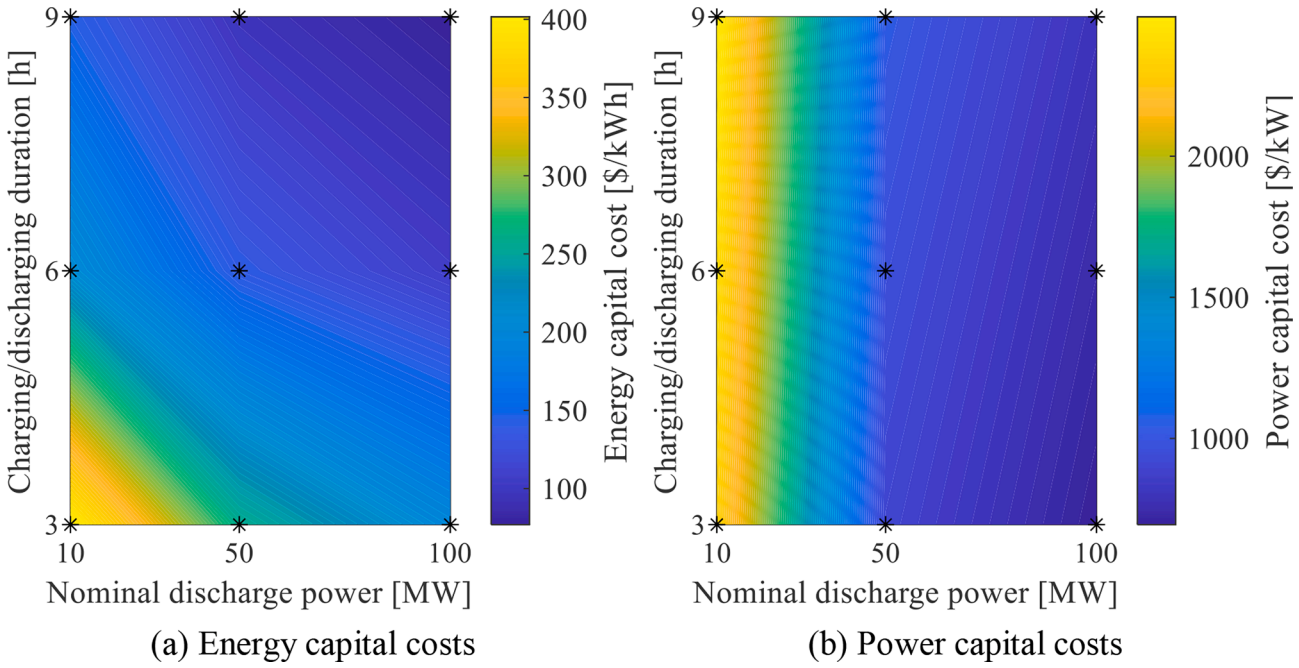

Fig. 5. Optimal (a) energy capital costs and (b) power capital costs of cost–optimal A–CAES systems at nominal discharge powers of 10 to 50 MW and charging/discharging durations of 3 to 9 h. The markers show the power-duration combinations for which the optimisations were performed, while the areas between the markers were interpolated.

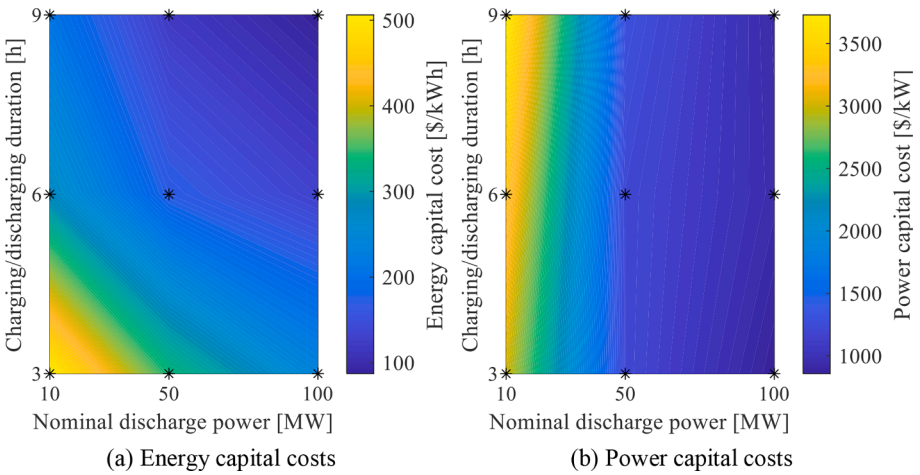

Fig. 6. Optimal (a) energy capital costs and (b) power capital costs of cost–optimal A–CAES systems with L-TESs at nominal discharge powers of 10 to 50 MW and charging/discharging durations of 3 to 9 h. The markers show the power-duration combinations for which the optimisations were performed, while the areas between the markers were interpolated.

Table 6
Comparison of the key performance indicators of the optimal A-CAES system with other potential large-scale electrical energy storage technologies, based on data from Olympios et al. [18] and Koohi–Fayegh and Rosen [11].

Technology	Energy capital cost [$/kWh]	Power capital cost [$/kW]	Roundtrip efficiency	Technology readiness level (TRL)
A-CAES	140	970	76%	5 [18]
Pumped-hydro storage	10–80 [18]	2,000–5,000 [18]	70–87% [18]	9 [18]
	5–100 [11]	500–4,600 [11]	50–90% [11]	
Liquid-air energy storage	200–600 [18]	900–6,000 [18]	43–62% [18]	7 [18]
Pumped-thermal energy storage	100–500 [18]	500–5,000 [18]	48–77% [18]	3–4 [18]
Li-ion batteries	600–4,000 [18]	1,000–4,000 [18]	70–90% [18]	9 [18]
	100–1,500 [11]	1,200–4,000 [11]	70–100% [11]	
VRB flow batteries	200–1,000 [18]	600–1,200 [18]	60–85% [18]	9 [18]
	150–1,000 [11]	600–1,500 [11]	60–90% [11]	

compare to alternative electrical energy storage technologies.

The energy capital cost of the cost-optimal A-CAES system are among the lowest of the compared technologies, only pumped-hydro storage can achieve about 90 $/kWh lower cost, while Li-ion and VRB flow batteries are on average 1,400 $/kWh and 450 $/kWh more expensive, respectively. The cost-optimal A–CAES system is also competitive in terms of power capital costs. The roundtrip efficiency is within the range of literature values for pumped-hydro storage, VRB flow batteries and Li-ion batteries, though the latter are on average 10% more efficient.

A-CAES systems have a lower technology readiness level than pumped-hydro storage, VRB flow batteries and Li-ion batteries, as commercial application is yet to be demonstrated. However, they use mature components, and commercial operation of diabatic CAES systems is well established.

3.5. Commercial challenges and opportunities

The study shows that A–CAES systems are a viable and cost–competitive solution for large–scale long–duration energy storage. The comparison presented in Table 6 shows that such systems are able to compete with other thermo–mechanical energy storage technologies and batteries both in terms of capital cost and roundtrip efficiency. However, while commercial operation of diabatic CAES systems has been established, A–CAES systems are still in demonstration stage and further commercial experience needs to be gained.

The study shows that, under the assumptions made, PB–TESs appear to be more favourable than L–TESs and should be prioritised for commercial systems. Further, it is demonstrated that a second thermal store improves the economics and efficiency compared to rejecting heat via an intercooler. Therefore, it is worth the added capital cost. The analysis also shows that lost–cost storage materials with a high specific heat capacity are favourable. For L–TESs, the temperature limit of the storage material plays an important role, as high temperatures are required to achieve high roundtrip efficiencies. Finally, the study shows strong economics of scale associated with the A–CAES systems. Commercial projects should therefore target large–scale systems to reduce specific energy and power capital costs.

While this study identifies least–cost designs of A–CAES systems, the commercial viability of these systems is not assessed. The latter will depend on the electricity price profile, specifically the average price paid for electricity for charging, and the revenue from electricity sales during discharging. Further revenue streams can include capacity reserve payments, negative electricity prices during times of high renewables availability, and subsidies.

One important assumption is the availability of a large salt cavern for air storage. If the air would have to be stored in tanks, the capital costs would increase significantly, and it would likely render large–scale projects infeasible. Additionally, operation with constant charging and discharging cycles is assumed. More dynamic operation, following electricity prices and renewables availability, should be assessed in future work, and for any commercial project.

4. Conclusions

A thermo-economic optimisation framework for adiabatic compressed-air energy storage (A–CAES) systems with either packed-bed thermal energy stores (PB-TESs) or liquid thermal energy stores (L–TESs) has been developed, and the performance of various system configurations with different storage materials has been investigated at different scales. System configurations include A–CAESs with one or two PB–TESs or L–TESs, while six different solid and six liquid thermal energy storage materials were considered (see Table 1 and Table 2). The results allow the comparison of different thermal energy storage technologies and materials as well as A-CAES system layouts based on thermodynamic and economic indicators. Optimal component sizes and operating parameters, which lead to the minimum energy capital cost, were identified for each configuration. The best–possible efficiencies and specific costs were calculated, which allows an estimation of the potential of A-CAES and a comparison to other large-scale energy storage technologies. The main novelty lies in the simultaneous optimisation of plant configuration, component sizing and operational parameters, with a focus on different TES systems and storage materials.

For a nominal discharge power of 50 MW and charging/discharging durations of 6 h, the optimal energy capital costs of systems with one PB–TES range from 150 to 200 $/kWh, depending on the storage material, with Basalt performing best. The corresponding power capital costs are between 1,050 and 1,440 $/kW, and roundtrip efficiencies between 47% and 54% are achieved by the cost-optimal system for each storage material. Systems with an L-TES have higher energy capital costs and lower roundtrip efficiencies. With solar salt, which is shown to be the best-performing liquid storage material, a minimum energy capital cost of 170 $/kWh and a power capital cost of 1,230 $/kW are reached at a roundtrip efficiency of 36%.

Adding a second thermal store instead of an intercooler improves the roundtrip efficiencies and reduces the costs of systems with PB-TESs. On average, the optimal energy capital costs are reduced by 8%, while the efficiencies of the cost-optimal systems improve by 26% points on average. The optimal energy capital costs of systems with L-TESs on the other hand only decrease for Rapeseed oil when adding a second thermal store, while for all other considered materials the costs increase. The roundtrip efficiency of the cost-optimal system, however, increases for all materials, on average by 15% points.

Overall, the best-performing A–CAES system in terms of energy capital cost was found to be the configuration with two PB–TESs with Basalt as storage material. For a nominal discharge power of 50 MW and charging/discharging durations of 6 h, an energy capital cost of 140 $/kWh and a power capital cost of 970 $/kW are achieved at a roundtrip efficiency of 76%.

A-CAES systems were found to benefit strongly from economies of scale. At a nominal discharge power of 100 MW and charging/discharging durations of 9 h, the optimal energy capital costs were found to be over 80% lower compared to a system with a nominal discharge power of 10 MW and charging/discharging durations of 3 h. Energy capital costs were found to decrease strongly with both, increasing nominal power and increasing charging/discharging time. Power capital costs on the other hand were found to depend most strongly on the nominal power, while the charging/discharging durations only have a secondary influence.

Since A-CAES systems use mature components and decades-long experience with operating diabatic CAES systems is available, A-CAES systems are ready to be deployed, at least as pilot plants, wherever sufficient underground storage volumes are available. Compared to literature values for other large-scale energy storage technologies, the energy capital costs of the optimal A-CAES system are about 90 $/kWh higher than those of pumped-hydro storage, but 450 $/kWh lower than those of VRB flow batteries and 1,400 $/kWh lower than those of Li–ion batteries. The power capital costs are among the lowest, comparable to those of pumped-hydro storage [11,18].

A cost breakdown by component reveals that the turbomachines (i.e., compressors, turbines) account for over three–quarters of total investment costs. Pressure vessel costs are significant for systems with PB–TESs, accounting for 9% of the total investment cost in the cost-optimal benchmark configuration. For systems with L-TESs, on the other hand, the storage material is the most significant other cost component, accounting for 13% of the total investment cost. Therefore, these components should be prioritised in efforts to reduce the costs of A-CAES systems. Another priority for future development should be raising the upper process temperature limits, as being able to attain higher temperatures was shown to improve performance and decrease specific costs. This could for example be achieved by using more advanced materials to construct the heat exchangers and thermal stores.

CRediT authorship contribution statement

Matthias Mersch: Methodology, Software, Validation, Formal analysis, Investigation, Data curation, Writing – original draft, Writing – review & editing, Visualization. **Paul Sapin:** Conceptualization, Methodology, Software, Validation, Writing – review & editing, Supervision. **Andreas V. Olympios:** Methodology, Data curation, Writing – review & editing. **Yulong Ding:** Writing – review & editing. **Niall Mac Dowell:** Resources, Writing – review & editing, Supervision. **Christos N. Markides:** Conceptualization, Methodology, Resources, Writing – review & editing, Supervision, Project administration, Funding acquisition.

Declaration of Competing Interest

The authors declare that they have no known competing financial interests or personal relationships that could have appeared to influence the work reported in this paper.

Data availability

Data will be made available on request.

Acknowledgements

This work was supported by the UK Engineering and Physical Sciences Research Council (EPSRC) [grant numbers EP/S032622/1, and EP/R045518/1]. Data supporting this publication can be obtained on request from cep-lab@imperial.ac.uk. For the purpose of Open Access, the authors have applied a CC BY public copyright licence to any Author Accepted Manuscript version arising from this submission.

References

[1] International Energy Agency (IEA), “Global Energy Review 2021,” Paris, 2021. [Online]. Available: https://www.iea.org/reports/global-energy-review-2021.
[2] Kondziella H, Bruckner T. Flexibility requirements of renewable energy based electricity systems – a review of research results and methodologies. Renew Sustain Energy Rev Jan. 2016;53:10–22. https://doi.org/10.1016/j.rser.2015.07.199.
[3] Lund PD, Lindgren J, Mikkola J, Salpakari J. Review of energy system flexibility measures to enable high levels of variable renewable electricity. Renew Sustain Energy Rev May 2015;45:785–807. https://doi.org/10.1016/j.rser.2015.01.057.
[4] Cruz MRM, Fitiwi DZ, Santos SF, Catalão JPS. A comprehensive survey of flexibility options for supporting the low-carbon energy future. Renew Sustain Energy Rev Dec. 2018;97:338–53. https://doi.org/10.1016/j.rser.2018.08.028.
[5] Arbabzadeh M, Sioshansi R, Johnson JX, Keoleian GA. The role of energy storage in deep decarbonization of electricity production. Nat Commun 2019;10(1):pp. https://doi.org/10.1038/s41467-019-11161-5.
[6] de Sisternes FJ, Jenkins JD, Botterud A. The value of energy storage in decarbonizing the electricity sector. Appl Energy 2016;175:368–79. https://doi.org/10.1016/j.apenergy.2016.05.014.
[7] Safaei H, Keith DW. How much bulk energy storage is needed to decarbonize electricity? Energy Environ Sci 2015;8(12):3409–17. https://doi.org/10.1039/c5ee01452b.
[8] Denholm P, Mai T. Timescales of energy storage needed for reducing renewable energy curtailment. Renew Energy Jan. 2019;130:388–99. https://doi.org/10.1016/j.renene.2018.06.079.

[9] Jafari M, Korpås M, Botterud A. Power system decarbonization: Impacts of energy storage duration and interannual renewables variability. Renew Energy 2020;156:1171–85. https://doi.org/10.1016/j.renene.2020.04.144.

[10] Chen H, Cong TN, Yang W, Tan C, Li Y, Ding Y. Progress in electrical energy storage system: A critical review. Prog Nat Sci 2009;19(3):291–312. https://doi.org/10.1016/j.pnsc.2008.07.014.

[11] Koohi-Fayegh S, Rosen MA. A review of energy storage types, applications and recent developments. J Energy Storage Feb. 2020;27:101047. https://doi.org/10.1016/j.est.2019.101047.

[12] Aneke M, Wang M. Energy storage technologies and real life applications – A state of the art review. Appl Energy 2016;179:350–77. https://doi.org/10.1016/j.apenergy.2016.06.097.

[13] Amirante R, Cassone E, Distaso E, Tamburrano P. Overview on recent developments in energy storage: Mechanical, electrochemical and hydrogen technologies. Energy Convers Manag 2017;132:372–87. https://doi.org/10.1016/j.enconman.2016.11.046.

[14] Gür TM. Review of electrical energy storage technologies, materials and systems: Challenges and prospects for large-scale grid storage. Energy Environ Sci 2018;11(10):2696–767. https://doi.org/10.1039/c8ee01419a.

[15] Luo X, Wang J, Dooner M, Clarke J. Overview of current development in electrical energy storage technologies and the application potential in power system operation. Appl Energy 2015;137:511–36. https://doi.org/10.1016/j.apenergy.2014.09.081.

[16] Görtz J, Aouad M, Terheiden K. Assessment of pumped hydropower energy storage potential along rivers and shorelines. Renew Sustain Energy Rev 2022. https://doi.org/10.1016/j.rser.2021.112027.

[17] Normyle A, Pittock J. A review of the impacts of pumped hydro energy storage construction on subalpine and alpine biodiversity: lessons for the Snowy Mountains pumped hydro expansion project. Aust Geogr 2020;51(1):pp. https://doi.org/10.1080/00049182.2019.1684625.

[18] Olympios AV, McTigue JD, Farres-Antunez P, Tafone A, Romagnoli A, Li Y, et al. Progress and prospects of thermo-mechanical energy storage—a critical review. Prog Energy Apr. 2021;3(2):022001. https://doi.org/10.1088/2516-1083/abdbba.

[19] Georgiou S, Shah N, Markides CN. A thermo-economic analysis and comparison of pumped-thermal and liquid-air electricity storage systems. Appl Energy 2018;226(June):1119–33. https://doi.org/10.1016/j.apenergy.2018.04.128.

[20] Georgiou S, Aunedi M, Strbac G, Markides CN. On the value of liquid-air and pumped-thermal electricity storage systems in low-carbon electricity systems. Energy Feb. 2020;193:116680. https://doi.org/10.1016/j.energy.2019.116680.

[21] White A, Parks G, Markides CN. Thermodynamic analysis of pumped thermal electricity storage. Appl Therm Eng 2013;53(2):291–8. https://doi.org/10.1016/j.applthermaleng.2012.03.030.

[22] McTigue JD, Farres-Antunez P, Markides CN, White AJ. Techno-economic analysis of recuperated Joule-Brayton pumped thermal energy storage. Energy Convers Manag 2022;252. https://doi.org/10.1016/j.enconman.2021.115016.

[23] Jadarizadeh H, Soltani M, Nathwani J. Assessment of the Huntorf compressed air energy storage plant performance under enhanced modifications. Energy Convers Manag Apr. 2020;209:112662. https://doi.org/10.1016/j.enconman.2020.112662.

[24] Budt M, Wolf D, Span R, Yan J. A review on compressed air energy storage: Basic principles, past milestones and recent developments. Appl Energy 2016;170:250–68. https://doi.org/10.1016/j.apenergy.2016.02.108.

[25] Kim YM, Lee JH, Kim SJ, Favrat D. Potential and evolution of compressed air energy storage: Energy and exergy analyses. Entropy 2012;14(8):1501–21. https://doi.org/10.3390/e14081501.

[26] Steinmann WD. Thermo-mechanical concepts for bulk energy storage. Renew Sustain Energy Rev 2017;75:205–19. https://doi.org/10.1016/j.rser.2016.10.065.

[27] Yirka B. SustainX builds 1.5 MW isotherm compressed air energy storage system. phys.org, 2013. https://phys.org/news/2013-09-sustainx-mw-isotherm-compressed-air.html (accessed Apr. 15, 2022).

[28] Bullough C, Gatzen C, Jakiel C, Koller M, Nowi A, Zunft S. Advanced Adiabatic Compressed Air Energy Storage for the Integration of Wind Energy. Proceedings of the European Wind Energy Conference, no. November. London, pp. 22–25, 2004, [Online]. Available: http://ewww.theeestory.com/files/EWEC_Paper_Final_2004.pdf.

[29] Grazzini G, Milazzo A. Thermodynamic analysis of CAES/TES systems for renewable energy plants. Renew Energy Sep. 2008;33(9):1998–2006. https://doi.org/10.1016/j.renene.2007.12.003.

[30] Hartmann N, Vöhringer O, Kruck C, Eltrop L. Simulation and analysis of different adiabatic Compressed Air Energy Storage plant configurations. Appl Energy 2012;93:541–8. https://doi.org/10.1016/j.apenergy.2011.12.007.

[31] Barbour E, Mignard D, Ding Y, Li Y. Adiabatic Compressed Air Energy Storage with packed bed thermal energy storage. Appl Energy 2015;155:804–15. https://doi.org/10.1016/j.apenergy.2015.06.019.

[32] Guo H, Xu Y, Chen H, Zhou X. Thermodynamic characteristics of a novel supercritical compressed air energy storage system. Energy Convers Manag 2016;115:167–77. https://doi.org/10.1016/j.enconman.2016.01.051.

[33] Bashiri Mousavi S, Adib M, Soltani M, Razmi AR, Nathwani J. Transient thermodynamic modeling and economic analysis of an adiabatic compressed air energy storage (A-CAES) based on cascade packed bed thermal energy storage with encapsulated phase change materials. Energy Convers Manag Sep. 2021;243:114379. https://doi.org/10.1016/j.enconman.2021.114379.

[34] Congedo PM, Baglivo C, Carrieri L. Hypothesis of thermal and mechanical energy storage with unconventional methods. Energy Convers Manag Aug. 2021;218:113014. https://doi.org/10.1016/j.enconman.2020.113014.

[35] Congedo PM, Baglivo C, Carrieri L. Application of an unconventional thermal and mechanical energy storage coupled with the air conditioning and domestic hot water systems of a residential building. Energy Build Oct. 2020;224:110234. https://doi.org/10.1016/j.enbuild.2020.110234.

[36] Razmi A, Soltani M, Tayefeh M, Torabi M, Dusseault MB. Thermodynamic analysis of compressed air energy storage (CAES) hybridized with a multi-effect desalination (MED) system. Energy Convers Manag Nov. 2019;199:112047. https://doi.org/10.1016/j.enconman.2019.112047.

[37] Alirahmi SM, Bashiri Mousavi S, Razmi AR, Ahmadi P. A comprehensive techno-economic analysis and multi-criteria optimization of a compressed air energy storage (CAES) hybridized with solar and desalination units. Energy Convers Manag May 2021;236:114053. https://doi.org/10.1016/j.enconman.2021.114053.

[38] Zhang X, Zeng R, Deng Q, Gu X, Liu H, He Y, et al. Energy, exergy and economic analysis of biomass and geothermal energy based CCHP system integrated with compressed air energy storage (CAES). Energy Convers Manag Nov. 2019;199:111953. https://doi.org/10.1016/j.enconman.2019.111953.

[39] Razmi R, Janbaz M. Exergoeconomic assessment with reliability consideration of a green cogeneration system based on compressed air energy storage (CAES). Energy Convers Manag Jan. 2020;204:112320. https://doi.org/10.1016/j.enconman.2019.112320.

[40] Soltani M, Nabat MH, Razmi AR, Dussealt MB, Nathwani J. A comparative study between ORC and Kalina based waste heat recovery cycles applied to a green compressed air energy storage (CAES) system. Energy Convers Manag Oct. 2020;222:113203. https://doi.org/10.1016/j.enconman.2020.113203.

[41] Vieira FS, Balestieri JAP, Matelli JA. Applications of compressed air energy storage in cogeneration systems. Energy Jan. 2021;214:118904. https://doi.org/10.1016/j.energy.2020.118904.

[42] Olabi AG, Wilberforce T, Ramadan M, Abdelkareem MA, Alami AH. Compressed air energy storage systems: Components and operating parameters – A review. J Energy Storage Feb. 2021;34:102000. https://doi.org/10.1016/j.est.2020.102000.

[43] King M, Jain A, Bhakar R, Mathur J, Wang J. Overview of current compressed air energy storage projects and analysis of the potential underground storage capacity in India and the UK. Renew Sustain Energy Rev Apr. 2021;139:110705. https://doi.org/10.1016/j.rser.2021.110705.

[44] Zhao Y, Song J, Liu M, Zhao Y, Olympios AV, Sapin P, et al. Thermo-economic assessments of pumped-thermal electricity storage systems employing sensible heat storage materials. Renew Energy Mar. 2022;186:431–56. https://doi.org/10.1016/j.renene.2022.01.017.

[45] Donadei S, Schneider G-S. Compressed Air Energy Storage in Underground Formations. In: Storing Energy. Elsevier; 2016. p. 113–33. https://doi.org/10.1016/B978-0-12-803440-8.00006-3.

[46] Bell IH, Wronski J, Quoilin S, Lemort V. Pure and Pseudo-pure Fluid Thermophysical Property Evaluation and the Open-Source Thermophysical Property Library CoolProp. Ind Eng Chem Res Feb. 2014;53(6):2498–508. https://doi.org/10.1021/ie4033999.

[47] Wilson DG. The Design of High-Efficiency Turbomachinery and Gas Turbines. 2nd edition. Upper Saddle River: Prentice Hall; 1998.

[48] Wang L, Lin X, Chai L, Peng L, Yu D, Liu J, et al. Unbalanced mass flow rate of packed bed thermal energy storage and its influence on the Joule-Brayton based Pumped Thermal Electricity Storage. Energy Convers Manag Apr. 2019;185:593–602. https://doi.org/10.1016/j.enconman.2019.02.022.

[49] Hewitt GF. Heat Exchanger Design Handbook 2008. Begellhouse; 2008.

[50] White AJ. Loss analysis of thermal reservoirs for electrical energy storage schemes. Appl Energy Nov. 2011;88(11):4150–9. https://doi.org/10.1016/j.apenergy.2011.04.030.

[51] Sciacovelli A, Li Y, Chen H, Wu Y, Wang J, Garvey S, et al. Dynamic simulation of Adiabatic Compressed Air Energy Storage (A-CAES) plant with integrated thermal storage – Link between components performance and plant performance. Appl Energy Jan. 2017;185:16–28. https://doi.org/10.1016/j.apenergy.2016.10.058.

[52] Löf GOG, Hawley RW. Unsteady-state heat transfer between air and loose solids. Ind Eng Chem Res 1948;40(6):1061–70.

[53] Sapin P, Simpson MC, Olympios AV, Mersch M, Markides CN. Cost-benefit analysis of reversible reciprocating-piston engines with adjustable volume ratio in pumped thermal electricity storage. In: ECOS 2020 - Proc. 33rd Int. Conf. Effic. Cost, Optim. Simul. Environ. Impact Energy Syst., June, pp. 1534–1545; 2020.

[54] Shu G, Li X, Tian H, Shi L, Wang X, Yu G. Design condition and operating strategy analysis of CO 2 transcritical waste heat recovery system for engine with variable

operating conditions. Energy Convers Manag Jun. 2017;142:188–99. https://doi.org/10.1016/j.enconman.2017.02.067.
[55] Rosner F, Yang D, Rao A, Samuelsen S. Technical note: Gas turbine price projection for n-th plant equipment cost. Eng Econ Mar. 2022:1–6. https://doi.org/10.1080/0013791X.2022.2048330.
[56] Ulrich GD, Vasudevan PT. Chemical engineering process design and economics : a practical guide. 2nd edition; 2004.
[57] Turton R. Analysis, synthesis, and design of chemical processes. 3rd ed. TS. Upper Saddle River, N.J: Prentice Hall; 2009.
[58] Seider WD, Lewin DR, Seader JD, Widagdo S, Gani R, Ng KM. Product and process design principles. 4th edition. New York: Wiley; 2017.
[59] Morandin M, Mercangöz M, Hemrle J, Maréchal F, Favrat D. Thermoeconomic design optimization of a thermo-electric energy storage system based on transcritical CO2 cycles. Energy Sep. 2013;58:571–87. https://doi.org/10.1016/j.energy.2013.05.038.
[60] Couper JR, Penney WR, Fair JR, Walas SM. Chemical process equipment: selection and design, Rev. 2nd e. London: Elsevier Butterworth-Heinemann; 2009.
[61] Chemical Engineering, The Chemical Engineering Plant Cost Index, 2022. https://www.chemengonline.com/pci-home (accessed Apr. 19, 2022).
[62] The MathWorks Inc., "surrogateopt," 2021. https://www.mathworks.com/help/gads/surrogateopt.html (accessed May 12, 2021).
[63] The MathWorks Inc., "fmincon Interior Point Algorithm," 2023. https://uk.mathworks.com/help/optim/ug/constrained-nonlinear-optimization-algorithms.html#brnpd5f (accessed Mar. 20, 2023).
[64] Baron H, Mukherjee R, Nathan VU, Garofanello M, Hamza M, Gaikwad S, et al. Static Equipment: Understanding Heat Exchangers. accessed Apr. 28, 2022 J Petrol Tech 2019. www.jpt.spe.org/static-equipment-understanding-heat-exchangers.